Check for updates

Tuning ferroelectric photovoltaic performance in *R*3*c*-CuNbO₃ through compressive strain engineering: a first-principles study

Zu-Da He, Wen-Ce Li, Jin-Long Yang, Hua-Kai Xu, Xiang-Fu Xu, Guo-Xia Lai, You-Da Che, Wei-Ling Zhu, Xiao-Dong Yang* and Xing-Yuan Chen [ID] *

Most ferroelectric oxides exhibit relatively wide bandgaps, which pose limitations on their suitability for photovoltaics application. CuNbO₃ possesses potential ferroelectric properties with an *R*3*c* polar structure that facilitate the separation of charge carriers under illumination, promoting the generation of photovoltaic effects. The optical and ferroelectric properties of *R*3*c*-CuNbO₃, as well as the effect of strain on the properties are investigated by first-principles calculation in this paper. The calculated results indicate that *R*3*c*-CuNbO₃ possesses a moderate band gap to absorb visible light. The interaction of Cu−O and Nb−O bonds is considered to have a crucial role in the photovoltaic properties of CuNbO₃, contributing to the efficient absorption of visible light. The bandgap of CuNbO₃ becomes smaller and the density of states near the conduction and valence bands becomes relatively uniform in distribution under compressive conditions, which improves the photoelectric conversion efficiency to 29.9% under conditions of bulk absorption saturation. The ferroelectric properties of CuNbO₃ are driven by the Nb−O bond interactions, which are not significantly weakened by the compressive strain. CuNbO₃ is expected to be an excellent ferroelectric photovoltaic material by modulation of compressive strain due to the stronger visible light absorption and excellent ferroelectric behavior.

1. Introduction

Oxide-group materials have wide potential application in ferroelectric, photocatalysis and photovoltaic fields.[1,2] Perovskite materials with *R*3*c* structure show a unique application prospect in the field of ferroelectric photovoltaics due to the internal electric field.[3,4] For example, BiFeO₃ and LiNbO₃ with *R*3*c* structure have internal ferroelectric polarization electric fields, which can promote carrier separation without the p–n junction.[5,6] Some ferroelectric oxides with a narrow band gap, such as Bi₂FeCrO₆, CuGaO₂, ABiO₃ (A = Ca, Cd, Zn, and Mg) and Pb(Fe₁/₂V₁/₂)O₃, exhibit strong visible light absorption, which is advantageous for achieving high photoconversion efficiency.[7–10] However, the band gap of most *R*3*c*-structured ferroelectric oxides is usually large and it is difficult for them to effectively absorb visible light.[11,12] Niobium oxide (CuNbOₓ) films have been shown to be excellent p-type semiconductors that can be stabilized as hole transport layers, significantly improving the efficiency of perovskite solar cells.[13] In addition, CuNbO₃ with perovskite structure is also considered as a potential semiconductor material for photovoltaic and photoelectrochemical conversion.[14] Narayanasamy successfully synthesized the *C*/2*m*

structure of CuNbO₃ by pulsed laser deposition technology, and applied it to dye-sensitized solar cells, achieving good photovoltaic performance.[15] First-principles calculations show that CuNbO₃ with *C*/2*m* structure can absorb visible light, and the optical properties are closely related to the Cu-d, Nb-d, and O-p energy level transitions.[16,17] At the same time, Fukuda *et al.* synthesized CuNbO₃ with an *R*3*c* structure, a polarized structural material with potential ferroelectric properties, although its light absorption properties have not been studied in detail.[18] In addition to the choice of materials, strain is also a key factor in regulating the physical properties of materials. Strain can induce and regulate changes in the physical properties of materials, such as ferroelectric depolarization, piezoelectricity, magnetoresistance, electrical capacitance, and photovoltaic performance.[19–22] By adjusting lattice parameters and electronic structure, strain can affect the band structure, ferroelectric polarization strength and optical properties to improve the photoelectric properties of the material.[23,24] The wide band gap ferroelectric oxides, such as BiFeO₃ (ref. 25) and InFeO₃,[26,27] have been shown to achieve significant bandgap adjustment while maintaining high ferroelectric polarization, which enhances the absorption of visible light and achieves excellent ferroelectric photovoltaic performance. In this paper, CuNbO₃ with an *R*3*c* structure has been investigated by density functional theory for the ferroelectric photovoltaic performance. The calculated result indicated that CuNbO₃ with an *R*3*c* structure is

Department of Physics, School of Science, Guangdong University of Petrochemical Technology, Maoming, Guangdong 525000, PR China. E-mail: chenxingyuan@gdupt.edu.cn; Fax: +86-668-2923567; Tel: +86-668-2923838

a new promising ferroelectric photovoltaic oxide. $CuNbO_3$ with an $R3c$ structure has a good ferroelectric polarization strength and can absorb visible light, which could improve the photovoltaic efficiency under the compressive strain conditions.

2. Computational method

All calculations in this paper are primarily conducted by using density functional theory implemented in the Vienna *Ab initio* Simulation Package (VASP) software, employing the pseudopotential plane wave method.[28,29] Exchange–correlation interactions are treated by using the Perdew–Burke–Ernzerhof (PBE) functional combined with Hubbard U correction (PBE+U).[30] The Hubbard U correction is particularly vital for the accurate calculation of the electronic structure with 3d transition metals.[31] The plane-wave cutoff is set at 550 eV, and the K-point sampling density within the Brillouin region is maintained at $0.03\ \text{Å}^{-1}$. The crystal structure was relaxed until the force acting on the atoms reached a magnitude lower than $0.001\ \text{eV}\,\text{Å}^{-1}$. The Hubbard U value for the Cu element in $R3c$-$CuNbO_3$ is set at 6 eV, with similar reports of Hubbard U correction available for other copper-based oxides.[17,32,33] The calculated results indicate that the band gap of $R3c$-$CuNbO_3$, obtained through the PBE+U approach, is approximately 1.7 eV. This value closely aligns with the band gap obtained using the HSE06 functional and is consistent with the experimental band gap of the $C/2m$ structure $CuNbO_3$.[14] Considering that the PBE+U method offers an accurate calculation of the electronic structure for 3d elemental materials and is more cost-effective, we have chosen to employ the PBE+U approach for subsequent calculations involving energy, electronic structure, band structure, ferroelectric and optical properties.

3. Calculation of the structure

The introduction of strain was achieved by simultaneous optimization of the ab-axis and c-axis lengths, as depicted in Fig. 1. The calculated results are summarized in Table 1. The calculated pristine $CuNbO_3$ lattice parameters are closed to the experimental values. $MgSnO_3$ and $LiNbO_3$ share structural similarities with $CuNbO_3$. With the possibility of growing $R3c$-$MgSnO_3$ films on $LiNbO_3$ substrates,[6,34] the lattice constant of $LiNbO_3$ (5.15 Å) was chosen to optimize the lattice parameters of $R3c$-$CuNbO_3$, introducing lattice strain. This choice is based on the smaller lattice constant of $LiNbO_3$ compared to $CuNbO_3$ (5.28 Å), leading to compressive strain within the $CuNbO_3$ lattice. Using the lattice parameter a of $LiNbO_3$ as a reference, the lattice parameter a and b of $R3c$-$CuNbO_3$ was adjusted to 5.15 Å through fitting, optimizing the lattice parameter c. The c-axis of $R3c$-$CuNbO_3$ under compressive strain (C–$CuNbO_3$) is changing from 14.22 Å to 14.55 Å. To assess mechanical stability under compressive strain, the strain stress method[35] within VASP software was employed to calculate the elastic constants of $CuNbO_3$ with the $R3c$ space group. Six independent elastic constants exist within the $R3c$ space group structure, including C_{11}, C_{12}, C_{13}, C_{14}, C_{33} and C_{44}. Based on the crystal mechanics stability criteria proposed by Mouhat and Coudert *et al.*,[36]

mechanical stability dictates that these independent elastic constants must adhere to specific inequalities.

$$C_{11} - C_{12} > 0,\ C_{11} + C_{12} > 0,\ C_{33} > 0,\ C_{44} > 0,\ (C_{11} + C_{12})C_{33} - 2C_{13}^2 > 0 \tag{1}$$

The calculated results, as presented in Table 2, confirm that both pristine $CuNbO_3$ and C–$CuNbO_3$ satisfy these inequalities, signifying their mechanical stability. The changes in the elastic constants of C–$CuNbO_3$ could be attributed to the compressive strain, which enhances the interatomic interactions, leading to bond shortening and an increase in the elastic constants. A similar situation exists for $R3c$-$InFeO_3$ and $R3c$-$MgSnO_3$ in our earlier research reports, where the compressive strain causes the bond length to become shorter resulting in a larger elastic constant.[27,37] Cu–O bond lengths are transitioned from 2.03 Å to 1.99 Å, whereas Nb–O bond lengths are changed from 2.14 Å to 2.12 Å under compressive strain in $R3c$-$CuNbO_3$.

4. Calculation of optical properties

The optical and electronic properties of the material are closely correlated with its band structure. As illustrated in Fig. 2(a) and (c), the calculated band gaps for pristine $CuNbO_3$ and C–$CuNbO_3$ are 1.7 eV and 1.50 eV, respectively, both of which are indirect band gaps. Notably, the band gap of $R3c$-$CuNbO_3$ closely aligns with the experimentally reported value for $C/2m$-structured $CuNbO_3$ (2.0 eV).[14] The band gap of $R3c$-$CuNbO_3$ is smaller compared to the ferroelectric materials with $R3c$ structure such as $BiFeO_3$ (2.7 eV),[38] $MgSnO_3$ (4.0 eV),[39] and $ZnSnO_3$ (3.7 eV).[39] It shares the potential for strong visible light absorption with narrow bandgap ferroelectric oxides like Bi_2FeCrO_6 (1.8 eV),[9] $CuGaO_2$ (1.46 eV),[8] and $ABiO_3$ (A = Ca, Cd, Zn, and Mg) (2.0 eV).[7] Under compressive conditions, the band gap of $R3c$-$CuNbO_3$ decreases to 1.50 eV. The valence band maximum of both pristine $CuNbO_3$ and C–$CuNbO_3$ (Fig. 2(b) and (d)) is primarily composed of Cu-3d orbitals and O-2p orbitals, while the conduction band minimum is predominantly occupied by Nb-4d orbitals and O-2p orbitals. The bonding states of Cu–O and the anti-bonding states of Nb–O play a pivotal role in the optical properties of $R3c$-structured $CuNbO_3$. The influence of compressive strain results in a reduction of the interatomic distance in C–$CuNbO_3$. The density of states (DOS) near the valence and conduction bands become relatively uniform distribution, resulting in a reduced bandgap and facilitating electron transitions. The band gap and dielectric function are intricately linked to the optical properties of the material. The optical properties can be obtained from the real (ε_1) and imaginary (ε_2) parts of the dielectric function within the Random Phase Approximation (RPA). The refractive index n and the extinction coefficient κ are determined from ε_1 and ε_2 with the photon energy E as follows.[40]

$$n(E) = \frac{1}{\sqrt{2}}\sqrt{\varepsilon_1(E) + \sqrt{\varepsilon_1{}^2(E) + \varepsilon_2{}^2(E)}} \tag{2}$$
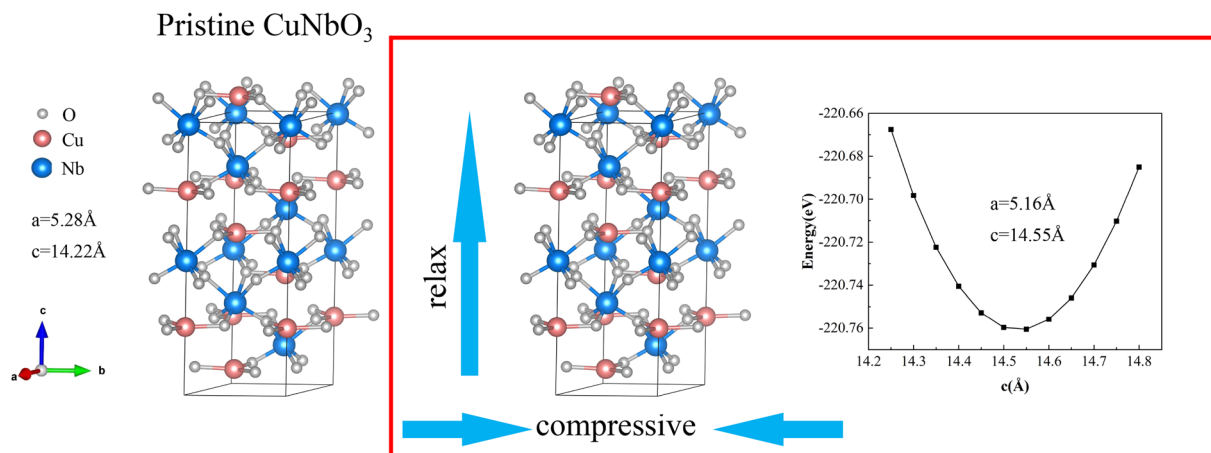
Pristine CuNbO₃

Fig. 1 The calculated structure of pristine and compressive $R3c$-CuNbO₃.

Table 1 The calculated and experimental lattice parameters

	a (Å)	b (Å)	c (Å)
CuNbO₃(exp)[14]	5.24	5.24	14.00
CuNbO₃ (cal)	5.28	5.28	14.22
C–CuNbO₃ (cal)	5.15	5.15	14.55

Table 2 The calculated elastic constants and the unit given in GPa

	C_{11}	C_{12}	C_{13}	C_{14}	C_{33}	C_{44}
CuNbO₃	204.167	138.897	88.539	6.668	193.172	31.948
C–CuNbO₃	236.263	171.384	104.460	4.204	216.713	31.433

$$\kappa(E) = \frac{1}{\sqrt{2}} \sqrt{-\varepsilon_1(E) + \sqrt{\varepsilon_1{}^2(E) + \varepsilon_2{}^2(E)}} \quad (3)$$

The reflectivity R and absorption α coefficient were calculated from n and κ.[40]

$$R(E) = \frac{(n-1)^2 + \kappa^2}{(n+1)^2 + \kappa^2} \quad (4)$$

$$\alpha(E) = \frac{4\pi\kappa}{hc/E} \quad (5)$$

Pristine $R3c$-CuNbO₃ exhibits a significant absorption coefficient within the visible light range, reaching 10^5 cm^{-1} in the Fig. 3a. In contrast, under compressive strain conditions, C–CuNbO₃ displays a reduced band gap and stronger absorption in the visible light range compared to pristine CuNbO₃, which is highly advantageous for photovoltaic applications. The photovoltaic conversion efficiency was estimated to evaluate photovoltaic potential of CuNbO₃. The following approach was employed to calculate the photovoltaic conversion efficiency (PCE).[41]

$$PCE = \frac{\int_0^{\lambda_{max}} W(\lambda)[1 - R(\lambda)]\left(1 - e^{-\alpha(\lambda)d}\right)C(\lambda)d\lambda}{\int_0^{\infty} W(\lambda)d\lambda} \quad (6)$$

Here, λ represents the wavelength of light, λ_{max} is the maximum absorption wavelength related to the band gap E_g as follows.

$$\lambda_{max} = \frac{hc}{E_g} \quad (7)$$

$W(\lambda)$ represents the solar spectrum irradiance (AM1.5), where d represents the thickness of the material. The calculated absorption α and reflectivity R coefficient are shown in the Fig. 3a and b. $C(\lambda)$ is the conversion factor, reflecting the ratio of photon energy converted to electron energy. It is related to the excitation energy of electron–hole pairs passing through the minimum band gap as follows.

$$C(\lambda) = \lambda \frac{E_g}{hc} \quad (8)$$

The calculated photovoltaic conversion efficiencies are illustrated in Fig. 3c. For pristine CuNbO₃ and C–CuNbO₃ with a thickness of 100 nm, the photovoltaic conversion efficiencies are 18.1% and 18.7%, respectively. The photovoltaic conversion efficiencies for pristine CuNbO₃ and C–CuNbO₃ with thickness of 500 nm are 25.6% and 27.5%, respectively. Both materials exhibit significantly high photovoltaic conversion efficiencies. The application of compressive strain further enhances the photovoltaic conversion efficiency of CuNbO₃ from 26.9% to 29.9% under conditions of bulk absorption saturation. The calculations of the optoelectronic properties suggest that $R3c$-CuNbO₃ is a promising photovoltaic material, with strain-induced enhancement of light absorption leading to increased photovoltaic conversion efficiency.

5. Calculation of ferroelectric properties

The ferroelectric polarization strength of both pristine CuNbO₃ and C–CuNbO₃ is determined by using the Berry phase method

(a)CuNbO₃ -Band structure

(b)CuNbO₃ -PDOS

(c)C-CuNbO₃ -Band structure

(d)C-CuNbO₃ -PDOS
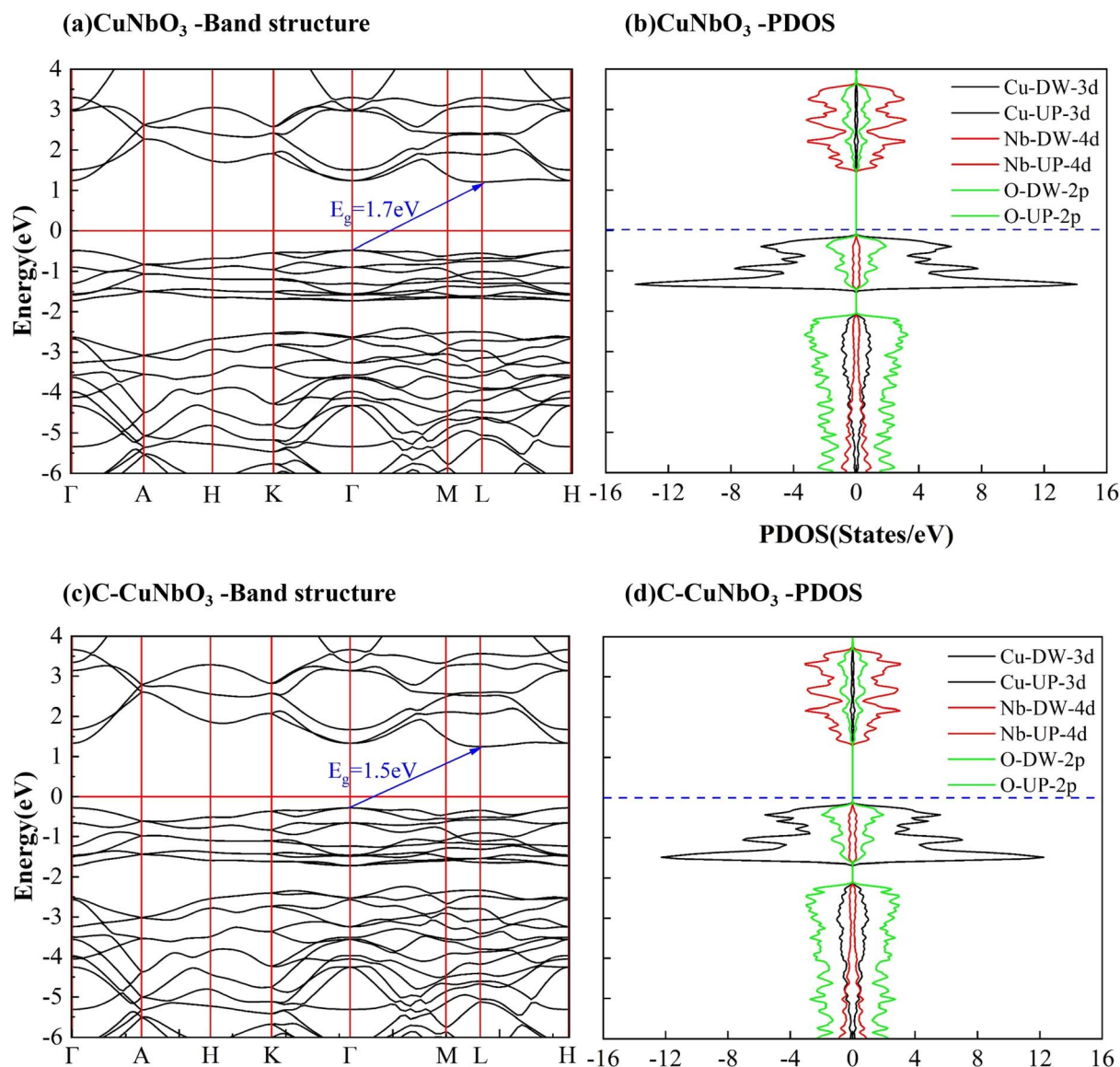

Fig. 2   The calculated energy band structure and partial density of states (PDOS) of (a and b) pristine and (c and d) compressive $R3c$-CuNbO₃.
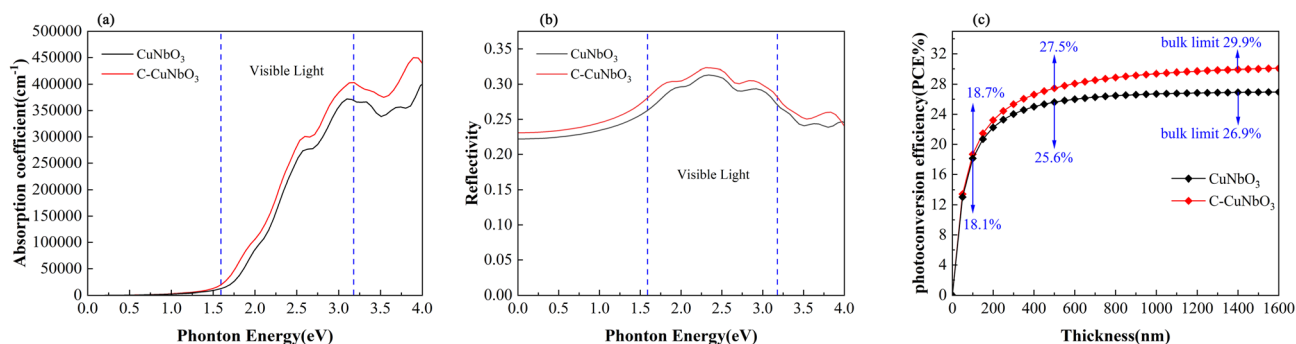

Fig. 3   The calculated (a) optical absorption coefficient, (b) reflection coefficient, and (c) photoelectric conversion efficiency. The range of visible light is indicated between the two dashed lines.
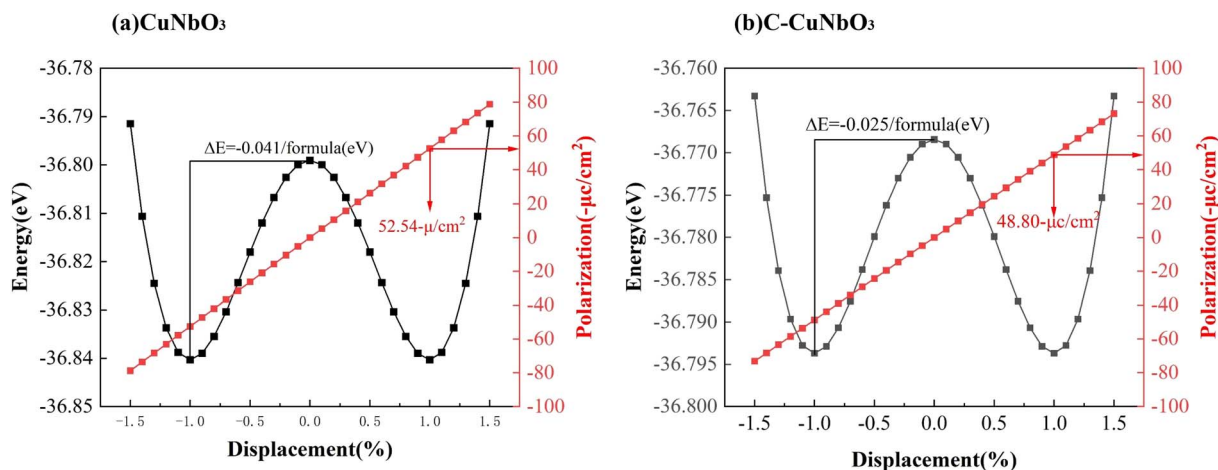
(a)CuNbO₃   (b)C-CuNbO₃

Fig. 4 The calculated ferroelectric polarization strength and energy changes as the atom interpolation shifts of (a) pristine and (b) compressive $R3c$-CuNbO₃.

Table 3 The calculated Born effective charges (e) and atomic offset (Å) away from centrosymmetric positions

		BEC_{xx}	BEC_{yy}	BEC_{zz}	Offset (Δz)
CuNbO₃	O	−2.98	−2.98	−2.80	−0.09
	Cu	1.05	1.05	1.09	0.01
	Nb	7.92	7.92	7.30	0.12
C–CuNbO₃	O	−2.99	−2.99	−3.02	−0.08
	Cu	0.93	0.93	1.03	−0.01
	Nb	8.03	8.03	8.04	0.10

within the framework of modern polarization theory.[42,43] As shown in Fig. 4, the $R3c$ space group is designated as the ferroelectric phase (state 1), while the centrosymmetric reference phase is labeled as $R\bar{3}c$ (state 0). The double-well potential energy curves and ferroelectric polarization strength are obtained by linearly interpolating between the centrosymmetric

phase (state 0) and the polar phase (state 1). These energy curves suggest that $R3c$-CuNbO₃ could exhibit promising ferroelectric properties similar to well-documented ferroelectric materials like BiFeO₃, ZnSnO₃ and MgSnO₃ in the literature.[44–46] Under compressive strain conditions, the ferroelectric polarization value of $R3c$-CuNbO₃ decreases from 52.54 μC cm⁻² to 48.80 μC cm⁻². In Table 3, the Born effective charges (BEC) and atomic displacements away from centrosymmetric positions are calculated to investigate the ferroelectric properties of CuNbO₃. Born effective charges quantify the induced dipole moment of an atom in response to a slight displacement from its equilibrium position caused by the applied electric field. Greater Born effective charges generally correspond to more pronounced polarization effects, indicating increased susceptibility to atomic displacement in response to an applied electric field. The calculated results reveal that the BEC of Nb is larger than that of Cu (1e+), at approximately 8e+, and this significantly contributes to the ferroelectric polarization of $R3c$-CuNbO₃. The
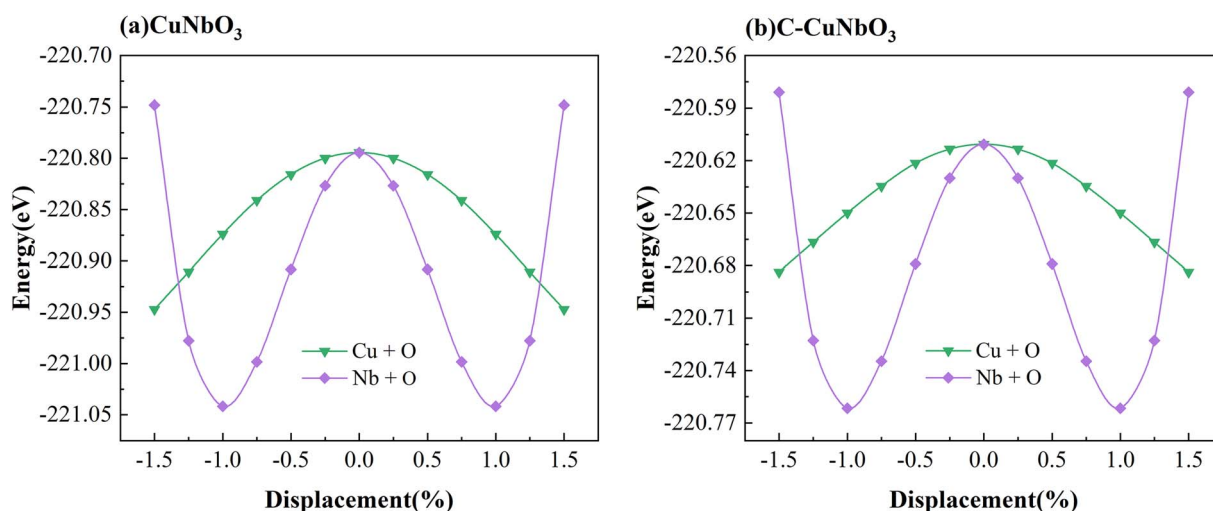
(a)CuNbO₃   (b)C-CuNbO₃

Fig. 5 The calculated energy changes as Cu−O and Nb−O movement of (a) pristine and (b) compressive $R3c$ CuNbO₃.

calculated displacements show relatively substantial movements of Nb and O atoms in $R3c$-CuNbO$_3$. Energy change diagrams for different atomic movements are also provided in Fig. 5, displaying a prominent double-well trend in atomic movement between Nb and O atoms, further affirming the pivotal role of Nb–O interaction in ferroelectric properties of $R3c$-CuNbO$_3$. In Table 3, it is observed that the offset for O in pristine CuNbO$_3$ is approximately 0.09 Å, while the Nb offset is about 0.12 Å. For C–CuNbO$_3$, the O offset is roughly 0.08 Å, and the Nb offset is approximately 0.10 Å. Under compressive strain conditions, the ferroelectric polarization strength of CuNbO$_3$ experiences a slight reduction due to the diminished displacement offsets. However, it still exhibits excellent ferroelectric properties, evident from the distinct double-potential well curve and robust ferroelectric polarization strength. The introduction of compressive strain in CuNbO$_3$ enhances its light absorption, coupled with outstanding ferroelectric behavior, rendering it a highly promising ferroelectric photovoltaic oxide material.

6. Conclusion

The optical and ferroelectric properties of $R3c$-CuNbO$_3$, as well as the impact of compressive strain, have been investigated by density functional theory. The calculated results showed that $R3c$-CuNbO$_3$ has a more suitable band gap for absorbing visible light compared to ferroelectric materials with the $R3c$ structure, such as BiFeO$_3$, ZnSnO$_3$, and MgSnO$_3$. The interactions between Cu–O and Nb–O bonds play a crucial role in establishing the favorable bandgap in $R3c$-CuNbO$_3$. The bandgap of $R3c$-CuNbO$_3$ decreased under compressive strain, leading to increased uniform distribution DOS near the valence and conduction bands, improving photovoltaic conversion efficiency to 29.9% under conditions of bulk absorption saturation. The photoelectric conversion efficiency of CuNbO$_3$ can be enhanced by the compressive strain interaction, without weakening its ferroelectric properties driven by Nb–O bond interactions. CuNbO$_3$ under compressive strain exhibits enhanced visible light absorption and retains its exceptional ferroelectric characteristics, leading to a promising ferroelectric photovoltaic material.

Conflicts of interest

The authors declared that they have no conflicts of interest to this work. We declare that we do not have any commercial or associative interest that represents a conflict of interest in connection with the work submitted.

Acknowledgements

References

1 J. He, Y. Liu, J. Qu, *et al.*, Boosting photocatalytic water oxidation on photocatalysts with ferroelectric single domains, *Adv. Mater.*, 2023, **35**(14), 2210374.

2 C. Gao, W. Li, L. Jing, *et al.*, Enhanced Fill Factor and Power Conversion Efficiency of Single Oxide Ferroelectric Photovoltaic Devices with Designed Nanostructures, *Adv. Funct. Mater.*, 2023, 2213178.

3 T. Choi, S. Lee, Y. J. Choi, *et al.*, Switchable ferroelectric diode and photovoltaic effect in BiFeO$_3$, *Science*, 2009, **324**(5923), 63.

4 X. Han, Y. Ji and Y. Yang, Ferroelectric photovoltaic materials and devices, *Adv. Funct. Mater.*, 2022, **32**(14), 2109625.

5 H. T. Yi, T. Choi, S. G. Choi, *et al.*, Mechanism of the switchable photovoltaic effect in ferroelectric BiFeO$_3$, *Adv. Mater.*, 2011, **23**(30), 3403.

6 C. Somma, K. Reimann, C. Flytzanis, *et al.*, High-field terahertz bulk photovoltaic effect in lithium niobate, *Phys. Rev. Lett.*, 2014, **112**(14), 146602.

7 J. He, C. Franchini and J. M. Rondinelli, Ferroelectric oxides with strong visible-light absorption from charge ordering, *Chem. Mater.*, 2017, **29**(6), 2445.

8 S. Song, D. Kim, H. M. Jang, *et al.*, β-CuGaO$_2$ as a strong candidate material for efficient ferroelectric photovoltaics, *Chem. Mater.*, 2017, **29**(17), 7596.

9 R. Nechache, C. Harnagea, S. Li, *et al.*, Bandgap tuning of multiferroic oxide solar cells, *Nat. Photonics*, 2015, **9**(1), 61.

10 Z. Wu, Y. Zhang, K. Ma, *et al.*, Strong visible-light photovoltaic effect in multiferroic Pb (Fe$_{1/2}$V$_{1/2}$)O$_3$ bulk ceramics, *Phys. Status Solidi RRL*, 2014, **8**(1), 36.

11 J. He, C. Franchini and J. M. Rondinelli, Lithium niobate-type oxides as visible light photovoltaic materials, *Chem. Mater.*, 2016, **28**(1), 25.

12 I. Grinberg, First-Principles Studies of Band Gap Engineering in Ferroelectric Oxides, *Isr. J. Chem.*, 2020, **60**(8–9), 823.

13 X. Ye, Z. Wen, R. Zhang, *et al.*, High-performance and stable inverted perovskite solar cells using low-temperature solution-processed CuNbOx hole transport layer, *J. Power Sources*, 2021, **483**, 229194.

14 U. A. Joshi, A. M. Palasyuk and P. A. Maggard, Photoelectrochemical investigation and electronic structure of a p-type CuNbO$_3$ photocathode, *J. Phys. Chem. C*, 2011, **115**(27), 13534.

15 P. Narayanasamy, S. G. Chidambaram, M. Mahendran, *et al.*, Fabrication of copper-niobium-oxygen complexes as a photocathode for p-type dye-sensitized solar cell, *Int. J. Energy Res.*, 2021, **45**(13), 19623.

16 M. Harb, D. Masih and K. Takanabe, Screened coulomb hybrid DFT investigation of band gap and optical absorption predictions of CuVO$_3$, CuNbO$_3$ and Cu$_5$Ta11O$_{30}$ materials, *Phys. Chem. Chem. Phys.*, 2014, **16**(34), 18198.

17 C. T. Crespo, $CuNbO_3$ as a solar energy converter to fuel and electricity, *Sol. Energy Mater. Sol. Cells*, 2018, **179**, 305.

18 M. Fukuda, I. Yamada, H. Murata, *et al.*, Perovskite-type $CuNbO_3$ exhibiting unusual noncollinear ferrielectric to collinear ferroelectric dipole order transition, *Chem. Mater.*, 2020, **32**(12), 5016.

19 Z. Wu, Y. Zhang, C. Fang, *et al.*, Magnetostriction-strain-induced enhancement and modulation of photovoltaic performance in Si-p–n/Tb_xD $y_{1-x}Fe_2$ composite, *Phys. Status Solidi A*, 2014, **211**(3), 641.

20 Y. Jia, X. Tian, J. Si, *et al.*, Modulation of strain, resistance, and capacitance of tantalum oxide film by converse piezoelectric effect, *Appl. Phys. Lett.*, 2011, **99**(1), 011905.

21 C. Fang, C. Wang, Z. Wu, *et al.*, Uniaxial stress-induced ferroelectric depolarization in <001>-oriented $0.72Pb(Mg_{1/3}Nb_{2/3})O_3$-$0.28PbTiO_3$ single crystal, *J. Alloys Compd.*, 2015, **647**, 14.

22 S. Gong, Z. Wu, Y. Jia, *et al.*, Strong strain modulation on magneto-resistance of $La_{0.85}Sr_{0.15}MnO_3$ film via converse piezoelectric effect, *J. Alloys Compd.*, 2018, **752**, 402.

23 D. Sando, Y. Yang, C. Paillard, *et al.*, Epitaxial ferroelectric oxide thin films for optical applications, *Appl. Phys. Rev.*, 2018, **5**(4), 041108.

24 D. Pesquera, E. Parsonnet, A. Qualls, *et al.*, Beyond substrates: strain engineering of ferroelectric membranes, *Adv. Mater.*, 2020, **32**(43), 2003780.

25 H. L. Liu, M. K. Lin, Y. R. Cai, *et al.*, Strain modulated optical properties in $BiFeO_3$ thin films, *Appl. Phys. Lett.*, 2013, **103**(18), 317.

26 J. S. Souza, L. L. Alves and A. F. Lima, Effects of tensile strain on the electronic, optical and ferroelectric properties of a multifunctional R3c $InFeO_3$ compound, *Comp. Mater. Sci.*, 2022, **215**, 111788.

27 X. F. Xu, G. X. Lai, K. R. Su, *et al.*, First-principles study on the elastic, electronic and photocatalytic properties of multiferroic material $InFeO_3$ under strain, *Int. J. Mod. Phys. B*, 2021, **35**(21), 2150215.

28 P. E. Blöchl, Projector augmented-wave Method, *Phys. Rev. B: Condens. Matter Mater. Phys.*, 1994, **50**, 17953.

29 G. Kresse and J. Furthmüller, Efficient iterative schemes for ab initio total-energy calculations using a plane-wave basis set, *Phys. Rev. B: Condens. Matter Mater. Phys.*, 1996, **54**, 11169.

30 A. I. Liechtenstein, V. I. Anisimov and J. Zaanen, Density-functional theory and strong interactions: Orbital ordering in Mott-Hubbard insulators, *Phys. Rev. B: Condens. Matter Mater. Phys.*, 1995, **52**(8), R5467.

31 H. J. Kulik, M. Cococcioni, D. A. Scherlis, *et al.*, Density functional theory in transition-metal chemistry: A self-consistent Hubbard U approach, *Phys. Rev. Lett.*, 2006, **97**(10), 103001.

32 M. Heinemann, B. Eifert and C. Heiliger, Band structure and phase stability of the copper oxides Cu_2O, CuO, and Cu_4O_3, *Phys. Rev. B: Condens. Matter Mater. Phys.*, 2013, **87**(11), 115111.

33 T. C. Sterling and D. Reznik, Effect of the electronic charge gap on LO bond-stretching phonons in undoped La_2CuO_4 calculated using LDA+U, *Phys. Rev. B: Condens. Matter Mater. Phys.*, 2021, **104**(13), 134311.

34 K. Fujiwara, H. Minato, J. Shiogai, *et al.*, Thin-film stabilization of LiNbO3-type $ZnSnO_3$ and $MgSnO_3$ by molecular-beam epitaxy, *APL Mater.*, 2019, **7**(2), 022505.

35 Y. Le Page and P. Saxe, Symmetry-general least-squares extraction of elastic data for strained materials from ab initio calculations of stress, *Phys. Rev. B: Condens. Matter Mater. Phys.*, 2002, **65**(10), 104104.

36 F. Mouhat and F. X. Coudert, Necessary and sufficient elastic stability conditions in various crystal systems, *Phys. Rev. B: Condens. Matter Mater. Phys.*, 2014, **90**(22), 224104.

37 X. F. Xu, *et al.*, Tuning mechanical properties, ferroelectric properties and electronic structure in R3c-$MgSnO_3$ by compressive strain: A first-principle study, *Phys. B*, 2021, **618**, 413143.

38 J. F. Ihlefeld, N. J. Podraza, Z. K. Liu, *et al.*, Optical band gap of $BiFeO_3$ grown by molecular-beam epitaxy, *Appl. Phys. Lett.*, 2008, **92**(14), 142908.

39 K. Fujiwara, H. Minato, J. Shiogai, *et al.*, Thin-film stabilization of LiNbO3-type $ZnSnO_3$ and $MgSnO_3$ by molecular-beam epitaxy, *APL Mater.*, 2019, **7**(2), 022505.

40 M. Fox, *Optical Properties of Solids*, 2002.

41 G. Shi and E. Kioupakis, Electronic and optical properties of nanoporous silicon for solar-cell applications, *ACS Photonics*, 2015, **2**(2), 208.

42 R. Resta, Macroscopic polarization in crystalline dielectrics: the geometric phase approach, *Rev. Mod. Phys.*, 1994, **66**(3), 899.

43 N. A. Spaldin, A beginner's guide to the modern theory of polarization, *J. Solid State Chem.*, 2012, **195**, 2.

44 J. B. Neaton, C. Ederer, U. V. Waghmare, *et al.*, First-principles study of spontaneous polarization in multiferroic $BiFeO_3$, *Phys. Rev. B: Condens. Matter Mater. Phys.*, 2005, **71**(1), 014113.

45 J. Zhang, K. L. Yao, Z. L. Liu, *et al.*, First-principles study of the ferroelectric and nonlinear optical properties of the LiNbO3-type $ZnSnO_3$, *Phys. Chem. Chem. Phys.*, 2010, **12**(32), 9197.

46 X. Y. Chen, J. Q. Tan, K. R. Su, *et al.*, First-principles study of R3c-$MgSnX_3$ (X=O, S and Se) for photovoltaic and ferroelectric application, *Phys. Lett. A*, 2022, **422**, 127774.